Short-time diffusivity of dicolloids

Mark M. Panczyk, Norman J. Wagner, and Eric M. Furst*
Department of Chemical and Biomolecular Engineering and Center for Molecular and Engineering Thermodynamics, Allan P. Colburn Laboratory, 150 Academy Street, University of Delaware, Newark, Delaware 19716, USA
(Received 3 March 2014; published 25 June 2014)

The short-time diffusivity of dicolloid particles as a function of particle volume fraction ϕ from $0.01 \leqslant \phi \leqslant 0.6$ is measured using diffusing wave spectroscopy. The diffusivities of symmetric and asymmetric dicolloids are compared with similarly sized spheres. The short-time diffusivity is independent of salt concentration and decreases with increasing volume fraction for both spheres and asymmetric dicolloids. Symmetric dicolloids have a higher diffusivity than spheres at similar volume fractions. This difference is accounted for by rescaling the dicolloid volume fraction based on the ratio of the random close-packing volume fractions of spheres and dicolloids. Finally, a useful method is provided for calculating the diffusivity of symmetric dicolloid particles of arbitrary aspect ratio based on the calculated hydrodynamic resistance of Zabarankin [Proc. R. Soc. A **463**, 2329 (2007)].

DOI: 10.1103/PhysRevE.89.062311 PACS number(s): 82.70.Dd, 05.40.Jc, 78.35.+c, 47.85.Dh

I. INTRODUCTION

The rich equilibrium phase behavior of uniform anisotropic particles is a source of continued interest in colloid science in part because they offer new possibilities for self-assembled structures [1–3]. Dicolloids, particles in the shape of two fused spheres, are particularly interesting because they can be assembled into a variety of structures depending on their concentration and the presence of applied directing fields, including face-centered-cubic, hexagonally close-packed, triclinic, base-centered-monoclinic, and body-centered-tetragonal crystals [4,5]. In two dimensions, dicolloids in electric fields form open, centered rectangular two-dimensional structures belonging to the *c2mm* and *p2* plane groups [6,7]. In addition to these many phases, which include one of the highest packing densities of uniform colloidal particles, crystals of dicolloid particles have been shown to exhibit rich structural color and photonic band-gap properties [8–10]. The annealing of defects, mechanical properties, and melting of dicolloid crystals is also significantly distinct from that of crystals of spherical particles [11–14].

Despite many reports of dicolloid particle assembly, there are comparatively few studies of their dynamics. Such data are useful in determining the kinetics of assembly [10], especially as particles are concentrated to form ordered or disordered close-packed structures and consequently experience a slowing of their dynamics. Although the glass and gel transitions of dicolliods have been recently studied by rheology [15] and mode coupling theory [16], and Stokesian dynamics simulations have been used to calculate the short-time translational and rotational dynamics of dicolloid particles [17], experimental measurements of the dynamics of these anisotropic particles remain unexplored.

Diffusing wave spectroscopy (DWS) [18–20] has been used to measure the dynamics of concentrated suspensions of spheres [21–24] and is used here to determine the short-time diffusivity of dicolloid particles as the particle volume fraction increases. On the short length and time scales probed by DWS, the motion of a colloidal particles is a function of its hydrodynamic interactions only [25,26]. The suspension structure does not relax or reconfigure appreciably. Investigating the short-time dynamics provides a method of determining the hydrodynamic interactions of the particles independent of thermal forces, and therefore provides insight to particle mobility, high frequency rheology, and the kinetics of self-assembly.

This article begins by reviewing the particle synthesis, characterization, and preparation, followed by a description of the dynamic light scattering and diffusing wave spectroscopy experimental methods. Measurements of the diffusivity of spheres, asymmetric dicolloids, and symmetric dicolloids are then discussed. In the Appendix, we provide a method for determining the diffusivity of dicolloid particles based on the calculated hydrodynamic resistance based on a numerical interpolation of Zabarankin's hydrodynamic calculations [27].

II. METHODS

A. Materials

Crosslinked latex spheres and dicolloids are synthesized using seeded emulsion polymerization [28–31]. Symmetric and asymmetric dicolloids were synthesized from crosslinked latex seed particles by first swelling them with monomer and then initiating a second polymerization reaction upon heating. As the monomer is ejected, it partially wets the seed particle and polymerizes into a second lobe. The anisotropy and asymmetry are controlled by the cross-linking density and amount of monomer added. The particle dimensions were determined using scanning electron microscopy (see Fig. 1). The radius of the seed spheres is $a = 1.44 \pm 0.05$ μm; the asymmetric dicolloids have a length $L = 4.4 \pm 0.1$ μm and diameters of $d_1 = 3.3 \pm 0.1$ μm and $d_2 = 3.8 \pm 0.1$ μm. The symmetric dicolloids have a length of $L = 4.3 \pm 0.1$ μm and diameter of $d = 3.3 \pm 0.1$ μm. Their aspect ratios are $\alpha = L/\bar{d} - 1 = 0.24 \pm 0.01$ and 0.33 ± 0.01 for the

*furst@udel.edu

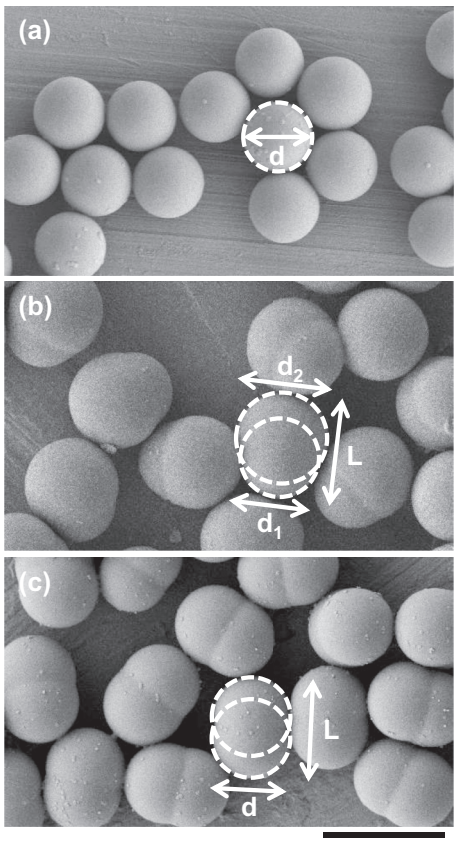

FIG. 1. SEM images of (a) spheres, (b) asymmetric dicolloids, and (c) symmetric dicolloids. The scale bar corresponds to 5 μm.

asymmetric and symmetric dicolloids, respectively, where $\bar{d} = d$ for symmetric dicolloids and $\bar{d} = (d_1 + d_2)/2$ for the asymmetric particles. The volume of the asymmetric particles is $V = 32.8\ \mu\text{m}^3$ and the volume of the symmetric particles is $V = 26.8\ \mu\text{m}^3$. A useful characteristic length scale, the radius of a sphere with the same volume as the dicolloids, is $a_{\text{eff}} = (3V/4\pi)^{1/3} = 1.99\ \mu$m for asymmetric dicolloids and 1.86 μm for symmetric dicolloids.

The colloidal particles are dispersed in a 10^{-3}-M solution of the surfactant hexaetheylene glycol monododecyl ether ($C_{12}E_6$, Sigma, catalog number 52044-1G, lot number BCBB7464V) and ultrapurified water (minimum resistivity 18.2 MΩ cm). The particles are then treated to remove impurities by centrifuging and replacing the supernatant five times with a 10^{-4}M solution of $C_{12}E_6$ in ultrapurified water, 0.1 mM or 3 mM potassium chloride (KCl, Alfa Aesar Puratronic 99.997% metals basis, Stock number 10839, Lot 28287). The Debye length in solutions with ionic strength I, $\kappa^{-1} = (\epsilon\epsilon_0 k_B T/2N_{av}e^2 I)^{1/2}$, is $\kappa^{-1} \approx 200$ nm for solutions without added salts, and 30 nm and 5.6 nm, for 0.1 mM and 3 mM KCl solutions, respectively. The electrophoretic mobilities of spheres, asymmetric dicolloids, and symmetric dicolloids measured at a salt concentration of 0.1 mM KCl were -1.76 ± 0.03, -3.21 ± 0.04, and -2.34 ± 0.03 (μm/s)/(V/cm), respectively (ZetaPALS, Brookhaven Instruments Corporation). These mobilities are consistent with surface potentials on the order of -30mV.

The target volume fraction of suspensions is prepared by first centrifuging the particles and assuming the cake at the bottom is at random close packing. This cake is then diluted to the desired volume fraction. The reported concentration is determined by drying and weighing a 200-500 μL sample of the suspension.

B. Dynamic light scattering

Dynamic light scattering (DLS) measurements were performed with a 632.8 nm vacuum wavelength laser (using a BI-200SM goniometer version 2.0, Brookhaven Instruments). Dilute sphere, asymmetric dicolloid and symmetric dicolloid suspensions ($\phi \approx 0.001\%$) were prepared and the intensity autocorrelation function was measured at the scattering angle $\theta = 20^\circ$ using a digital correlator (Brookhaven BI-9000AT). The intensity autocorrelation function is converted to the field autocorrelation function using the Siegert relation

$$\frac{\langle I(t)I(t+t_d)\rangle}{\langle I(t)\rangle^2} = g_2(t_d) = 1 + \beta\,|g_1(q,t_d)|^2 \qquad (1)$$

where β is the dynamical contrast factor that is an instrument-dependent parameter. The field autocorrelation function is

$$g_1(t) = \exp[-q^2 D_0 t] \qquad (2)$$

where D_0 is the single-particle self-diffusivity. In the experiment $q = \frac{4\pi n}{\lambda}\sin(\frac{\theta}{2}) = 4.59\ \mu\text{m}^{-1}$. Equation 2 is fit to experimental data to determine the infinite dilution diffusivity of the particles.

C. Diffusing wave spectroscopy

A diffusing wave spectroscopy (DWS) apparatus operating in a plane-wave transmission geometry was constructed following the standard methods [32]. A vertically polarized, argon ion laser operating at a vacuum wavelength $\lambda = 514.5$ nm (Coherent Innova-90C-5) is expanded and focused on a cuvette with a path length of either 4 mm (Plastibrand semimicrocuvettes, cat. no. 7591 50) or 1 mm (Implen Dilucell 10, batch no. B-230811) containing the suspended particles. The transmitted light passes through a horizontally polarized plate to eliminate light that has not been depolarized by multiple scattering. A collimated fiber optic collects the scattered light, which is split between two photomultiplier tubes (Model BI-CCDS, Brookhaven Instruments) before the cross correlation is taken using the digital correlator. Cross correlation reduces detector noise caused by dark current and after pulsing.

As in DLS, the Siegert relation [Eq. (1)] is used to determine the field autocorrelation function. In the transmission geometry, the field correlation function for a plane wave incident source is

$$g_1(t) = \frac{(L/l^* + 4/3)\sqrt{k_0^2\langle\Delta r^2(t)\rangle}}{\sinh(L/l^* + 4/3)\sqrt{k_0^2\langle\Delta r^2(t)\rangle}}, \qquad (3)$$

where the scattering wave vector is $k_0 = 2\pi n/\lambda$ in a medium with refractive index n [24]. The concentration-dependent mean transport path for the photons, l^*, is equal to the mean separation of particles when their diameter is small

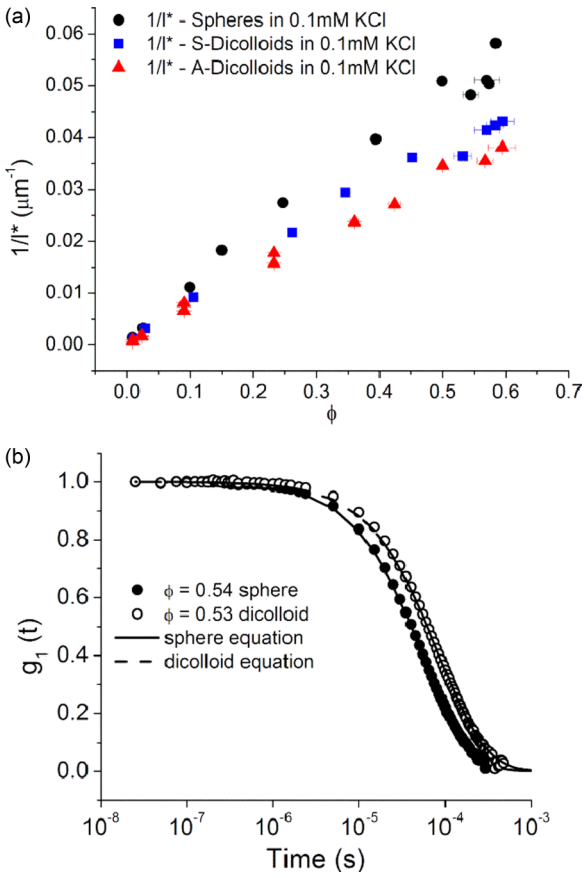

FIG. 2. (Color online) (a) Inverse of the mean transport path l^* of spheres, symmetric dicolloids, and asymmetric dicolloids plotted as a function of volume fraction. (b) Autocorrelation functions of spheres and symmetric dicolloids with fits using Eq. (3).

and scattering is isotropic. However, scattering from larger particles and interactions between particles strongly influences the diffuse light transport [18]. We find l^* by first measuring the transmission intensity of a 0.989-μm diameter latex sphere standard (Polybead polystyrene microspheres 2.63% solids, catalog number 07310, standard deviation $\sigma = 0.02$ μm) with known diffusivity. The reference photon transport length l^*_{ref} is determined from the autocorrelation function and Eq. (3). The value for l^* for the dicolloid samples is experimentally determined using the equation [18]

$$l^* = \frac{T l^*_{\mathrm{ref}}}{T_{\mathrm{ref}} + \frac{4 l^*_{\mathrm{ref}}}{3L}(T_{\mathrm{ref}} - T)}, \tag{4}$$

in which T_{ref} and l^*_{ref} are the transmission intensity and mean transport path of the standard and T is the transmission intensity of the particle dispersion. The measured l^* is plotted in Fig. 2(a) for all particle shapes at 0.1 mM KCl. Other salt concentrations follow the same trend. Using the Einstein relation, $\langle \Delta r^2(t) \rangle = 6Dt$, the diffusivity of each sample is found by a nonlinear least-squares fit.

III. RESULTS AND DISCUSSION

A. Light transport and field autocorrelation

The DWS field autocorrelation function [Eq. (3)] describes the light scattering data when changes in the light transport in the samples are properly characterized as the particle volume fraction increases. The decay of the correlation corresponds to the characteristic time needed for the particles to diffuse a root-mean-squared distance similar to $\langle \Delta r^2 \rangle^{1/2} = l^*/k_0 L$ [32]. With increasing particle concentration, l^* decreases as the distance between scattering events decreases. Simultaneously, the relaxation time increases since the particle motion slows. Equation (3) accounts for both changes by using the independently measured l^* to obtain the diffusivity $D(\phi)$ of the suspended particles.

In Fig. 2(a), the values of l^* for spheres, asymmetric dicolloids, and symmetric dicolloids are shown with particle volume fraction. For spheres, the scattering mean-free path length ranges from $l^* \approx 850$ μm at the most dilute conditions to $l^* \approx 17$ μm at the highest concentration. Symmetric and asymmetric dicolloids follow this general trend, with a slightly lower value ($l^* \approx 25$ μm) at the highest concentrations. The value of l^* is related to the particle scattering form factor $P(q)$ and scattering structure factor $S(q)$ by

$$l^* = k_0{}^{-6} \left(\pi \rho \int_0^{2k_0} P(q) S(q) q^3 dq \right)^{-1} \tag{5}$$

and therefore reflects differences in the scattering properties of the anisotropic particles and their arrangement with increasing concentration compared with spheres [24].

With the measured l^* values, the particle root-mean-squared displacement ranges from $\langle \Delta r^2 \rangle^{1/2} \approx 13$ nm for $L = 4$ mm and $l^* = 850\,\mu$m to $\langle \Delta r^2 \rangle^{1/2} \approx 1$ nm for $L = 1$ mm and $l^* = 25\,\mu$m. The small displacements relative to the particle size $\langle \Delta r^2 \rangle^{1/2}/a \leqslant 10^{-3}$, and average interparticle spacing, $\langle \Delta r^2 \rangle^{1/2}/(4\pi a^3/3\phi)^{1/3} \leqslant 10^{-3}$, confirm that DWS probes the short-time particle diffusivity. Examples of the the field autocorrelation functions $g_1(t)$ for spheres and dicolloids are shown in Fig. 2(b). The measured correlation functions are fit well by Eq. (3) using only D_0 as a fitting parameter. In the next section we report and discuss the values of D_0 with volume fraction for the three particle types.

B. Diffusivity

The diffusivity of a colloidal particle is expressed as the tensor quantity

$$\mathbf{D}_0 = kT\mathbf{R}^{-1}, \tag{6}$$

where $\mathbf{R}$ is a hydrodynamic resistance tensor that accounts for the viscous forces imparted on the undeformable particles,

$$\mathbf{R} = \begin{pmatrix} \mathbf{R}_{FU}, & \mathbf{R}_{F\Omega}, \\ \mathbf{R}_{LU}, & \mathbf{R}_{L\Omega} \end{pmatrix}. \tag{7}$$

Among the diagonal components of the matrix, $\mathbf{R}_{FU}$ is a tensor that relates the drag imposed by the translation due to an applied force $\mathbf{F}$ and $\mathbf{R}_{L\Omega}$ for rotation due to an applied torque $\mathbf{\Omega}$, while the off-diagonal contributions represent coupled

translation rotation, and are zero for axisymmetric particles [33].

For noninteracting spherical particles with radius a in a medium with viscosity η, an analysis of the Stokes equation gives

$$\mathbf{R}_{FU} = 6\pi a\eta\mathbf{I} \tag{8}$$

and

$$\mathbf{R}_{L\Omega} = 8\pi a^3\eta\mathbf{I}, \tag{9}$$

where $\mathbf{I}$ is the idem tensor. Thus, a sphere has an isotropic diffusivity, $\mathbf{D}_0 = D_0\mathbf{I}$, which is expressed in its scalar form as the familiar Stokes-Einstein-Sutherland relation,

$$D_0 = \frac{kT}{6\pi\eta a}. \tag{10}$$

The rotational diffusivity of uniform spheres does not contribute to the dynamic light scattering.

For anisotropic particles, the resistance depends on the motion of the particle relative to its orientation. For a uniaxially symmetric particle such as a dicolloid, with orientation of the major axis $\mathbf{d}$, the resistance tensor for translation must have the form

$$\mathbf{R}_{FU} = d_z\mathbf{dd} + d_x(\mathbf{I} - \mathbf{dd}), \tag{11}$$

where d_z and d_x are to be determined by solving the Stokes flow problem. DWS does not distinguish motion perpendicular or parallel to $\mathbf{d}$, so the translational diffusivity is the average of these components. For noninteracting particles

$$D_0 = \frac{2D_\perp^t + D_\parallel^t}{3}. \tag{12}$$

Likewise, the resistance tensor for rotation of an anisotropic particle has the form

$$\mathbf{R}_{L\Omega} = t_z\mathbf{dd} + t_x(\mathbf{I} - \mathbf{dd}). \tag{13}$$

Rotation is with respect to the longitudinal and equatorial axes, where t_z and t_x are constants again to be determined. Only rotation of the particle about the equatorial axis will factor into the scattering; however, due to the short time scales of motion measured using DWS, the rotational diffusivity of the dicolloid particles makes a negligible contribution to the correlation function and is omitted in the analysis. This can be shown by representing the dicolloid as two scattering centers separated by the length $l = L - d$. Over a time t, the rotation of the dicolloid particle about its equatorial axis sweeps the angle given by $\cos\theta(t) = \mathbf{d}(t)\cdot\mathbf{d}(0)$. The squared displacement of a scattering center Δr_c^2 that accompanies this rotation is

$$\Delta r_c^2 = \frac{l^2}{2}(1 - \cos\theta). \tag{14}$$

For small changes in the angle over short times, $\cos\theta \approx 1 - \theta^2/2$, and it follows that the effective diffusivity of the scattering center in units of length due to rotation is

$$D_{c,r} = (l^2/2)D_r. \tag{15}$$

In the Appendix, Zabarankin's solution to the Stokes flow of a dicolloid particle [27] is used to calculate the translational and rotational components of the diffusivity. For the symmetric dicolloid particle, which has the greatest anisotropy and therefore greatest contribution of rotational motion, the average translational diffusivity is $D_t = 0.114\,\mu\text{m}^2/\text{s}$, while the rotational diffusivity is $D_r = 0.022\,\text{rad}^2/\text{s}$ which gives $D_{c,r} = 0.0064\,\mu\text{m}^2/\text{s}$. The ratio of the time scales k_0^2/D_t and $k_0^2/D_{c,r}$ is 18, which shows that it takes more than an order of magnitude longer to observe a similar displacement due to rotation compared to translational motion.

Returning to the DWS experiments, the translational diffusivities of the three particle shapes studied, spheres, asymmetric dicolloids, and symmetric dicolloids, are calculated by fitting the transmission autocorrelation function using Eqs. (1) and (3). The data are shown in Figs. 3–5 for the three respective shapes. In each case, the diffusivity is normalized by the single particle self-diffusivity (the diffusivity at infinite dilution) measured using DLS. To highlight the trend of the diffusivity at higher particle concentrations, we plot the dimensionless ratio D_0/D against volume fraction.

In Fig. 3, the measured diffusivities of spheres are plotted alongside predictions for spheres from Stokesian dynamics simulations [35], the empirical equation by Lionberger and Russel [34] for spheres,

$$D(\phi)/D_0 = (1 - 1.56\phi)(1 - 0.27\phi), \tag{16}$$

as well as the translational diffusivity of spheres predicted by a modified Stokesian Dynamics simulation [17]. Equation (16) is known to agree well with the previous diffusivity measurements for spherical colloids by van Megan and Underwood [36] and Segré *et al.* [37]. These are all predictions for hard particles, however, the experimental data in Fig. 3 are the same regardless of the salt concentration, and hence the softness of the repulsive potential. This agreement confirms that the short-time diffusivity is a hydrodynamic quantity and is insensitive to the double-layer thickness for

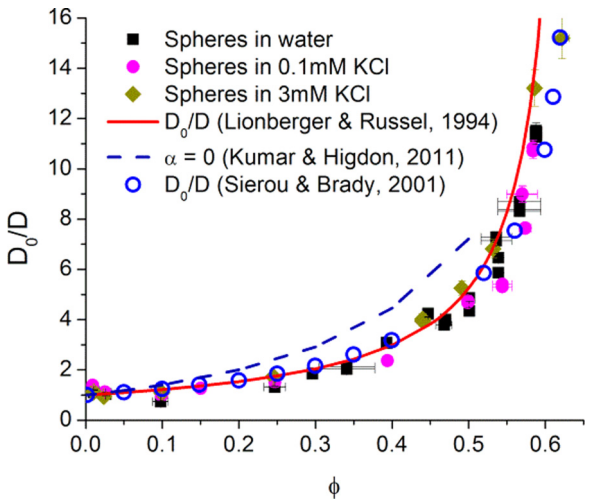

FIG. 3. (Color online) Diffusivity for spheres normalized by the measured diffusivity at infinite dilution. Also plotted is the Lionberger-Russel empirical correction for spheres [34], Stokesian Dynamics simulations for spheres by Sierou and Brady [35], and the translation component of the diffusivity of spheres from a modified Stokesian Dynamics simulation by Kumar and Higdon [17].

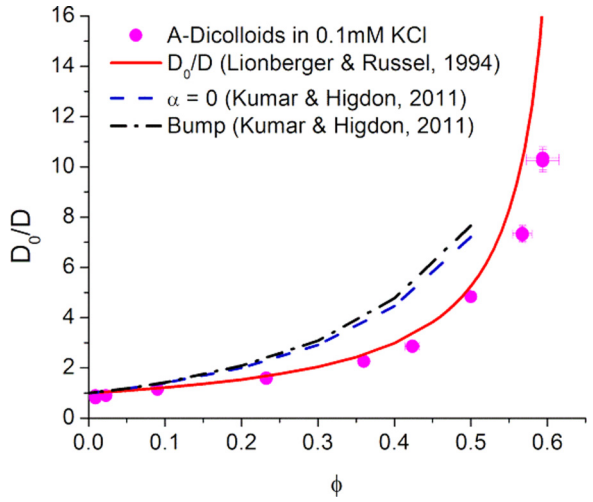

FIG. 4. (Color online) Diffusivity for asymmetric dicolloids using the radius of a sphere with the same volume and normalized using the measured diffusivity at infinite dilution from DLS. Also plotted is the Lionberger-Russel empirical prediction for spheres [34] and the translational diffusivity data from Stokesian dynamics simulations by Kumar and Higdon [17].

the salt concentrations studied, as shown previously [38,39]. The measured diffusivities are in excellent agreement with Eq. (16) and the values calculated by the Stokesian dynamics simulations of Sierou and Brady. The diffusivities calculated by the method of Kumar and Higdon are lower (and hence, the value D_0/D is higher) than the consensus values of prior experiments and simulations. As explained by Kumar and Higdon [17], this issue arises from the fact that the lubrication interactions used in their simulations are stronger than those used classically such as the simulations from Sierou and Brady.

The normalized short-time diffusivity for dicolloid particles are presented in Figs. 4 and 5 for asymmetric and symmetric particles, respectively. As for spheres, the diffusivity for each

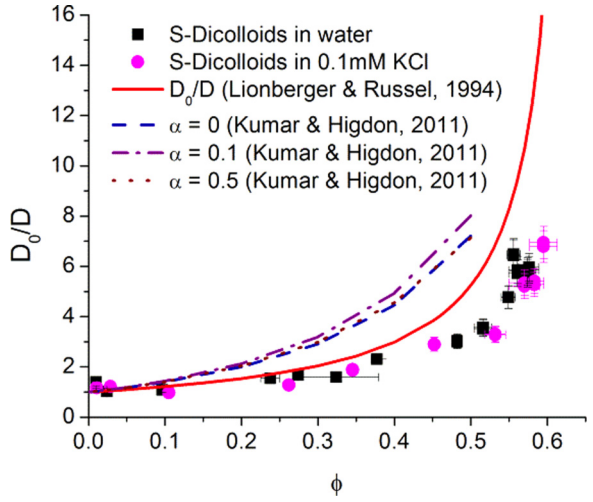

FIG. 5. (Color online) Diffusivity for symmetric dicolloids using the radius of a sphere with the same volume and and normalized using the measured diffusivity at infinite dilution from DLS.

dicolloid particle shape decreases with increasing volume fraction ϕ. Equation (16) is plotted as a reference in both figures.

The asymmetric particles have a lower aspect ratio (and a greater contrast in lobe diameters) than the symmetric dicolloids and therefore more closely resemble the shape of spherical particles. As shown in Fig. 4, the values of D_0/D closely follow the Lionberger-Russel equation for spheres. The diffusivities measured for asymmetric dicolloids are compared with the averaged translational and rotational diffusivity of a "bump" particles predicted by Kumar and Higdon in Fig. 4. The "bump" particle simulated has an aspect ratio $\alpha = L/\bar{d} - 1 = 0.22$ and lobe size difference of $\Delta d/\bar{d} = 0.22$. This compares to $\alpha = 0.24$ and $\Delta d/\bar{d} = 0.14$ for the asymmetric dicolloids used in this work. Similar to our experimental results, the simulations exhibit little difference between the comparable asymmetric dicolloids and spheres, despite the systematic deviation for all volume fractions noted previously.

For a given volume fraction, the diffusivity of symmetric dicolloids is higher than spheres, as seen in Fig. 5. Still, the diffusivity decreases significantly as the concentration increases. This trend is consistent with the theoretical prediction that dicolloids exhibit a glass transition at higher concentrations than spheres [40].

An explanation for the higher diffusivity of symmetric dicolloid particles is simply that they pack more efficiently than spheres or asymmetric dicolloids. The close-packed volume fraction of symmetric dicolloids with $\alpha = 0.33$ is $\phi^D_{CP} = 0.783$ [41], which is greater than the close-packed volume fraction of spheres, $\phi^S_{CP} = 0.740$. The greater distance between particles for symmetric dicolloids as compared to spheres at the same volume fraction leads to lower hydrodynamic resistance to motion for the dicolloids. An analogous argument can be made by comparing the random-close packing of spheres versus symmetric dicolloids, which better represents

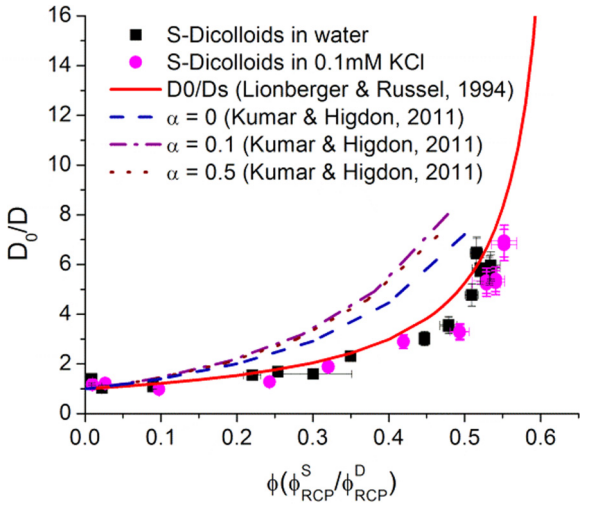

FIG. 6. (Color online) The volume fraction is normalized by the ratio of the ϕ_{RCP} for spheres and dicolloids. Also plotted is the Lionberger-Russel empirical prediction for spheres [34] and the translational diffusivity data from Stokesian dynamics simulations by Kumar and Higdon [17].

the structure expected in these experiments as the volume fraction increases. The random close packing for dicolloids with $\alpha = 0.33$ is $\phi^D_{\mathrm{RCP}} \approx 0.69$ [10], compared to the value for spheres, $\phi^S_{\mathrm{RCP}} = 0.64$.

The idea that the close packing or random close packing volume fractions can account for differences in the short-time diffusivity leads to the following surprising rescaling of the experimental data for symmetric dicolloids: simply multiplying the symmetric dicolloid volume fraction by the ratio $\phi^S_{\mathrm{RCP}}/\phi^D_{\mathrm{RCP}} = 0.64/0.69 = 0.93$ collapses the diffusivity of the anisotropic particles onto the empirical expression for spheres. Figure 6 shows the resulting normalized data are in excellent agreement with theory, simulation, and experiment (by comparison with Fig. 3) for the diffusivity of spheres.

IV. CONCLUSIONS

In this work, DWS was used to measure the short-time dynamics of dicolloid particles in solution. The method was verified by comparing the dynamics measured for spheres to theoretical predictions. The short-time behavior was independent of salt concentration within the range of ionic strengths studied. The short-time self-diffusivity of "bump" asymmetric dicolloids was indistinguishable from spheres. Symmetric dicolloids were less hindered by hydrodynamic interactions than spheres at comparable ϕ, which can be rationalized by the effects of particle shape on maximum packing. The short-time diffusivity of symmetric dicolloids can therefore be directly compared to spherical particles if the volume fractions are normalized by ratio of volume fractions at random close packing.

ACKNOWLEDGMENTS

We acknowledge J. Swan for helpful discussions. This work was supported by the National Science Foundation (Grant No. CBET-0930549).

APPENDIX: DICOLLOID PARTICLE SELF-DIFFUSIVITY

For symmetric dicolloids, the diffusivity at infinite dilution can be calculated based on the hydrodynamic resistance matrices reported by Zabarankin [27]. Zabarankin analyzed the Stokes flow equations by representing the velocity in the form of Dean and O'Neill [42] and solving the resulting integral equations for several particle aspect ratios, α. Here, we provide a numerical method using these resistance values to calculate the symmetric dicolloid short-time diffusivity for any dicolloid aspect ratio.

First, tables of the dimensionless resistance coefficients provided by Zabarankin are fit to quadratic functions with respect to the aspect ratio, as shown in Fig. 7. The fits are within 0.41% of their tabulated values, and give

$$\begin{aligned} d'_x &= d'_y = -0.105\alpha^2 + 0.554\alpha + 1.0005, \\ d'_z &= -0.067\alpha^2 + 0.356\alpha + 1.0002, \\ t'_x &= t'_y = 1.13\alpha^2 + 1.60\alpha + 1.003, \\ t'_z &= -0.368\alpha^2 + 1.174\alpha + 0.999. \end{aligned} \tag{A1}$$

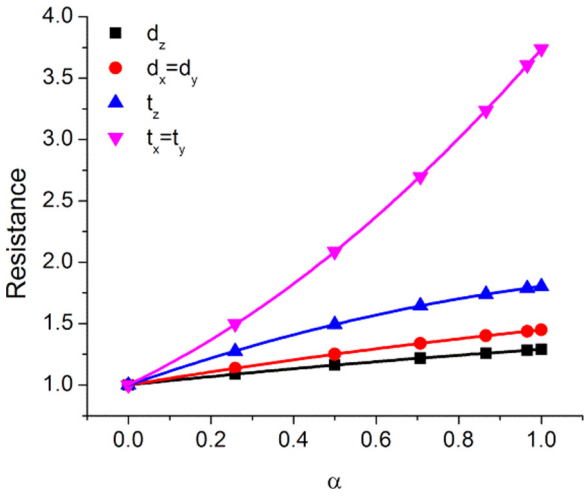

FIG. 7. (Color online) Plot of the four resistance coefficients calculated by Zabarankin [27] and their corresponding quadratic fits from Eq. (A1).

The resistance parameters calculated in Eq. (A1) can be used to determine the diffusivities due to translation

$$D^t_\perp = \frac{kT}{6\pi\eta a d'_x}, \tag{A2}$$

$$D^t_\parallel = \frac{kT}{6\pi\eta a d'_z}, \tag{A3}$$

and rotation

$$D^r_\perp = \frac{kT}{8\pi\eta a^3 t'_x}, \tag{A4}$$

$$D^r_\parallel = \frac{kT}{8\pi\eta a^3 t'_z}, \tag{A5}$$

where $2a$ is the diameter of the spherical lobes. Notably, $D^r_\parallel$, the rotation along the axis of symmetry, is not detected in light scattering experiments. Weighing and averaging the relevant diffusive moments from the light scattering experiment, the infinite dilution diffusivity is given by Eq. (12).

The single particle diffusivity can be calculated both by using the diffusivity of an equivalent volume sphere (D^V_0), as well as from Eqs. (A1), (A5), and (12) for the symmetric dicolloids (D^{Zab}_0). The error here is propagated from the error in the measured particle size. It can also be measured using DLS (D^{DLS}_0). A comparison of the diffusivities at infinite dilution at 20 °C are presented in Table I. The measured and calculated values for the diffusivity are within error of the measurements for the spheres and the asymmetric dicolloids; however, there is a slightly larger difference for the symmetric dicolloids. This is understandable since (D^V_0) should only be viewed as an approximation for anisotropic particles and using the method above yields much better agreement with the experimental diffusivity data. The percentages in parentheses correspond to the difference of the calculated diffusivity to the measured diffusivity. Given the small difference between

TABLE I. Diffusivities at infinite dilution calculated using the radius of an equivalent volume sphere, measured using DLS and calculated using Eqs. (A1), (A5), and (12). Deviations of the calculated values from the measured values using DLS are shown in parentheses.

Particle	D_0^V (μm^2/s)	D_0^{DLS} (μm^2/s)	D_0^{Zab} (μm^2/s)
Sphere	0.149 ± 0.005 (-1.9%)	0.152 ± 0.002	
A-Dicolloid	0.108 ± 0.003 (-0.2%)	0.108 ± 0.003	
S-Dicolloid	0.116 ± 0.003 (10.3%)	0.105 ± 0.009	0.114 ± 0.003 (9.2%)

the measured and calculated values, there is little qualitative difference between the choice of the infinite dilution diffusivity D_0, although there can be a quantitative difference up to 10% in the case of the symmetric dicolloids.

[1] S. C. Glotzer and M. J. Solomon, Nat. Mater. **6**, 557 (2007).
[2] M. Grzelczak, J. Vermant, E. M. Furst, and L. M. Liz-Marzán, ACS Nano **4**, 3591 (2010).
[3] S. Sacanna, D. J. Pine, and G.-R. Yi, Soft Mater. **9**, 8096 (2013).
[4] M. Marechal and M. Dijkstra, Phys. Rev. E **77**, 061405 (2008).
[5] A. F. Demirörs, P. M. Johnson, C. M. van Kats, A. van Blaaderen, and A. Imhof, Langmuir **26**, 14466 (2010).
[6] I. D. Hosein and C. M. Liddell, Langmuir **23**, 10479 (2007).
[7] M. M. Panczyk, J.-G. Park, N. J. Wagner, and E. M. Furst, Langmuir **29**, 75 (2013).
[8] I. D. Hosein, B. S. John, S. H. Lee, F. A. Escobedo, and C. M. Liddell, J. Mater. Chem. **19**, 344 (2009).
[9] I. D. Hosein, S. H. Lee, and C. M. Liddell, Adv. Funct. Mater. **20**, 3085 (2010).
[10] J. D. Forster, J.-G. Park, M. Mittal, H. Noh, C. F. Schreck, C. S. O'Hern, H. Cao, E. M. Furst, and E. R. Dufresne, ACS Nano **5**, 6695 (2011).
[11] S. J. Gerbode, S. H. Lee, C. M. Liddell, and I. Cohen, Phys. Rev. Lett. **101**, 058302 (2008).
[12] S. J. Gerbode, U. Agarwal, D. C. Ong, C. M. Liddell, F. Escobedo, and I. Cohen, Phys. Rev. Lett. **105**, 078301 (2010).
[13] S. J. Gerbode, D. C. Ong, C. M. Liddell, and I. Cohen, Phys. Rev. E **82**, 041404 (2010).
[14] U. Agarwal and F. A. Escobedo, Soft Mater. **8**, 5916 (2012).
[15] R. C. Kramb and C. F. Zukoski, J. Phys.: Condens. Matter **23**, 035102 (2011).
[16] R. Zhang and K. S. Schweizer, J. Chem. Phys. **133**, 104902 (2010).
[17] A. Kumar and J. J. L. Higdon, J. Fluid Mech. **675**, 297 (2011).
[18] D. A. Weitz and D. J. Pine, in *Dynamic Light Scattering*, edited by W. Brown (Oxford University Press, New York, 1993), pp. 652–720.
[19] G. Maret and P. E. Wolf, Z. Phys. B: Condens. Matter **65**, 409 (1987).
[20] D. J. Pine, D. A. Weitz, P. M. Chaikin, and E. Herbolzheimer, Phys. Rev. Lett. **60**, 1134 (1988).
[21] X. Qiu, X. L. Wu, J. Z. Xue, D. J. Pine, D. A. Weitz, and P. M. Chaikin, Phys. Rev. Lett. **65**, 516 (1990).
[22] S. Fraden and G. Maret, Phys. Rev. Lett. **65**, 512 (1990).
[23] P. D. Kaplan, A. G. Yodh, and D. J. Pine, Phys. Rev. Lett. **68**, 393 (1992).
[24] L. F. Rojas-Ochoa, S. Romer, F. Scheffold, and P. Schurtenberger, Phys. Rev. E **65**, 051403 (2002).
[25] I. Snook, W. Vanmegen, and R. J. A. Tough, J. Chem. Phys. **78**, 5825 (1983).
[26] J. F. Brady, J. Chem. Phys. **99**, 567 (1993).
[27] M. Zabarankin, Proc. R. Soc. A **463**, 2329 (2007).
[28] H. R. Sheu, M. S. Elaasser, and J. W. Vanderhoff, J. Pol. Sci. Part A **28**, 653 (1990).
[29] E. B. Mock, H. De Bruyn, B. S. Hawkett, R. G. Gilbert, and C. F. Zukoski, Langmuir **22**, 4037 (2006).
[30] J. W. Kim, R. J. Larsen, and D. A. Weitz, J. Am. Chem. Soc. **128**, 14374 (2006).
[31] J.-G. Park, J. D. Forster, and E. R. Dufresne, J. Am. Chem. Soc. **132**, 5960 (2010).
[32] D. J. Pine, D. A. Weitz, J. X. Zhu, and E. Herbolzheimer, J. Phys. (France) **51**, 2101 (1990).
[33] É. Guazzelli and J. F. Morris, *A Physical Introduction to Suspension Dynamics* (Cambridge University Press, New York, 2012).
[34] R. A. Lionberger and W. B. Russel, J. Rheol. **38**, 1885 (1994).
[35] A. Sierou and J. F. Brady, J. Fluid Mech. **448**, 115 (2001).
[36] W. van Megen and S. M. Underwood, J. Chem. Phys. **91**, 552 (1989).
[37] P. N. Segre, O. P. Behrend, and P. N. Pusey, Phys. Rev. E **52**, 5070 (1995).
[38] J. X. Zhu, D. J. Durian, J. Müller, D. A. Weitz, and D. J. Pine, Phys. Rev. Lett. **68**, 2559 (1992).
[39] J. Bergenholtz, F. M. Horn, W. Richtering, N. Willenbacher, and N. J. Wagner, Phys. Rev. E **58**, R4088 (1998).
[40] R. Zhang and K. S. Schweizer, Phys. Rev. E **80**, 011502 (2009).
[41] C. Vega, E. P. A. Paras, and P. A. Monson, J. Chem. Phys. **96**, 9060 (1992).
[42] W. R. Dean and M. E. O'Neill, Mathematika **10**, 13 (1963).